Photonic heat transport from weak to strong coupling

Minh Tam ⬤, George Thomas ⬤, and Dmitry S. Golubev

Pico group, QTF Centre of Excellence, Department of Applied Physics, Aalto University, 00076 Aalto, Finland

Superconducting circuits provide a favorable platform for quantum thermodynamic experiments. An important component for such experiments is a heat valve, i.e., a device which allows one to control the heat power flowing through the system. Here we theoretically study the heat valve based on a superconducting quantum interference device (SQUID) coupled to two heat baths via two resonators. The heat current in such a system can be tuned by magnetic flux. We investigate how the heat current modulation depends on the coupling strength g between the SQUID and the resonators. In the weak coupling regime the heat current modulation grows as g^2, but, surprisingly, at the intermediate coupling it can be strongly suppressed. This effect is linked to the resonant nature of the heat transport at weak coupling, where the heat current dependence on the magnetic flux is a periodic set of narrow peaks. At the intermediate coupling the peaks become broader and overlap, thus reducing the heat modulation. At very strong coupling the heat modulation grows again and finally saturates at a constant value.

I. INTRODUCTION

Quantum thermodynamics attracts a lot of attention both from the fundamental physics viewpoint and due to potential applications in nanoscale devices [1–3]. In this context, understanding of the heat transport in nanoscale systems is very important [4–10]. Precise control and tuning of the heat power is essential for the design of quantum heat engines [11–17], thermal rectifiers [18–21], transistors [22–25], masers [26], and circulators [17]. Such thermal devices can also be used for heat management in quantum circuits [10,27]. According to the theory [28,29], the heat current carried by quasiparticles can be controlled by magnetic flux in properly designed superconducting circuits. Such tunability of the quasiparticle heat current has been successfully demonstrated in the experiments with proximized normal metals [25,30–32] and with Josephson tunnel junctions [33,34]. Alternatively, one can use a magnetic flux tunable superconducting quantum interference device (SQUID) loop with two Josephson junctions to control the heat carried by photons propagating through the electric circuit. The SQUID may either operate as a classical inductor [35–37] or as a qubit [9,38,39]. At very low temperatures the photonic heat flux usually dominates over the phononic and the quasiparticle contributions [40]. In addition, this mechanism permits heat transmission over macroscopic distances [37] and remote management of the heat. In such devices the heat current can be accurately measured employing, for example, the normal metal–insulator–superconductor junctions as thermometers [41].

Here we theoretically study the photonic heat transport in the superconducting heat valve similar to the one used in the experiment [38]; see Fig. 1. It consists of the two resistors kept at different temperatures, two resonators, and the SQUID loop tunable by magnetic flux. We extend the results of Refs. [9,38], where several limiting cases have been already considered, and study the heat transport at arbitrary coupling between the SQUID and the resonators. To find the

heat current in the system we use the Landauer formalism for the heat transport (see, e.g., the review [5]). In the context of nanoelectronic systems the Landauer formula for the heat current can be derived from the Langevin equations for the fluctuating Josephson phase [42] coupled to the Nyquist noise of the resistors [43]. The Landauer formalism is standard for this type of problem; it has been used, for example, in Refs. [9,22,44], etc. The advantage of this approach is the possibility of studying both weak and strong coupling regimes. In the past, thermodynamics of systems weakly coupled to the environment has been studied extensively, and there also have been many extensions of the theory to the strong coupling regime [45–49]. One of the difficulties in this context is the ambiguity in the definition of heat at strong coupling [50]. Here we express the heat in terms of the temperature changes of the metallic islands playing the role of thermal baths. Thus, in our model, the heat is defined via the changes of the internal energies of the baths. This definition is inspired by the experiments mentioned above and the heat defined in this way can be experimentally measured regardless of the coupling strength between the SQUID and the resonators.

The device depicted in Fig. 1 operates as a heat valve and allows one to tune the heat flux between the resistors by changing the critical current of the SQUID with the magnetic flux. From the practical point of view, the performance of the valve is characterized by the heat current modulation amplitude, i.e., by the difference between the maximum and the minimum values of the heat current. We investigate how the heat modulation varies with various system parameters and obtain two surprising results. First, we find that the modulation of the heat depends on the coupling strength between the SQUID and the resonators in a nonmonotonous way. Indeed, the modulation grows with the coupling strength in the weak coupling regime, it almost vanishes at the intermediate coupling, then it grows again and eventually saturates at very strong coupling. Second, the strongest heat modulation is
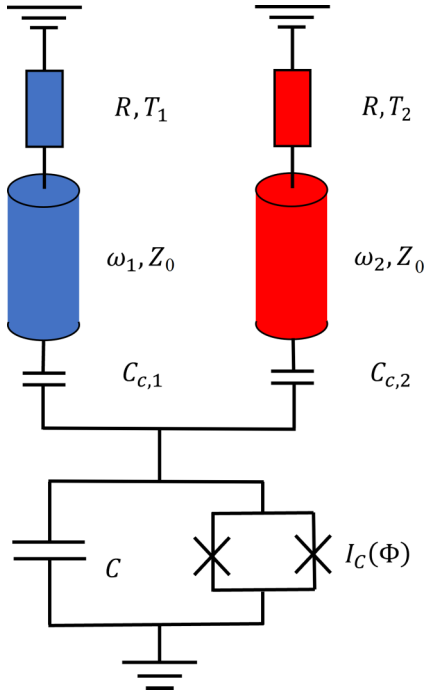
FIG. 1. Schematics of the heat valve under consideration. The hot bath is indicated by red color and the cold one by blue color. The two baths are realized as two transmission line resonators terminated by two resistors having the same resistance R and kept at temperatures T_1, T_2. The resonators have the same characteristic impedance Z_0 and the frequencies of the fundamental modes $\omega_{1,2}$. They are coupled to the SQUID loop via the capacitors $C_{c,1}, C_{c,2}$. The dc SQUID is characterized by the capacitance of the tunnel junctions C and by the Josephson critical current $I_C(\Phi)$ (1), which depends on the external magnetic flux Φ threading the SQUID.

achieved in the weak coupling regime. In our modeling we use feasible parameters [38,51,52] and we believe that our predictions can be experimentally tested. Finally, we have derived analytical expressions for the heat flux in various limiting cases in terms of the circuit parameters.

We organize the paper as follows: in Sec. II we introduce the model, in Sec. III we qualitatively discuss our main findings, in Secs. IV–VI we analytically analyze the weak, the intermediate, and the strong coupling regimes, and in Sec. VII we summarize the results. The derivation of the Landauer formula for the heat current is given in the Appendix.

II. MODEL

We consider an electric circuit depicted in Fig. 1. In this circuit, the two normal metal islands, having the same resistances R and kept at constant temperatures T_1, T_2, act as heat baths. The temperatures T_j ($j = 1, 2$) can be experimentally monitored using biased normal metal–insulator–superconductor junctions [41]. The two identical superconducting coplanar waveguide $\lambda/4$ resonators with characteristic impedance Z_0 serve as filters. The resonators are coupled to the SQUID via the capacitors $C_{c,j}$. The frequencies of the resonators ω_1 and ω_2 may slightly differ to compensate the difference between C_{c1} and C_{c2}, as we explain below.

In this setup, the SQUID can act as a heat valve [10,38]. Indeed, it provides a control parameter, the external magnetic field, which one can use to tune the heat current through the system. We assume that the symmetric SQUID is made of the two identical Josephson tunnel junctions and its critical current I_C periodically depends on the magnetic flux Φ as

$$I_C(\Phi) = I_{C,0}|\cos(\pi\Phi/\Phi_0)|. \tag{1}$$

Here $I_{C,0}$ is the critical current at zero flux and Φ_0 is the magnetic flux quantum. The SQUID is characterized by the Josephson energy $E_J(\Phi) = \hbar I_C(\Phi)/2e$ and by the charging energy $E_C = e^2/2(C_{c,1} + C_{c,2} + C)$, where C is the capacitance of the tunnel junctions of the SQUID; see Fig. 1. Here we consider the limit $E_J(0) \gg E_C$ and $E_C \lesssim k_B T_j \lesssim 2E_J(0)$. In this case, the Josephson junctions of the SQUID, which are nonlinear elements, can be approximately replaced by a linear inductor $L_J(\Phi) \approx \hbar/2eI_C(\Phi)$ and the SQUID as a whole by an LC circuit with the frequency

$$\omega_J(\Phi) = \sqrt{8E_J(\Phi)E_C}/\hbar. \tag{2}$$

To describe the transport of heat by photons between the resistors 1 and 2, we use the quasiclassical Langevin equation where the power spectra of Nyquist noises generated by the resistors are determined by the fluctuation-dissipation theorem [42]. In this way, we obtain the following expression for the heat current from the resistor 2 to the resistor 1 [43] (see also Appendix):

$$J(\Phi) = \int_0^\infty d\omega \frac{\hbar\omega}{2\pi}\tau(\omega, \Phi)[N_2(\omega) - N_1(\omega)]. \tag{3}$$

Here $N_j(\omega) = 1/(e^{\hbar\omega/k_B T_j} - 1)$ are the Bose functions and $\tau(\omega, \Phi)$ is the transmission probability, which depends on frequency and magnetic flux. Equation (3) has the familiar form of the Landauer formula for the photon current [5]. For the circuit of Fig. 1 the transmission probability $\tau(\omega, \Phi)$ is given by [9,43]

$$\tau(\omega, \Phi) = \frac{4\,\mathrm{Re}\left[\frac{1}{Z_1(\omega)}\right]\mathrm{Re}\left[\frac{1}{Z_2(\omega)}\right]}{\left|-i\omega C + \frac{1}{Z_1(\omega)} + \frac{1}{Z_2(\omega)} + \frac{1}{Z_J(\omega,\Phi)}\right|^2}, \tag{4}$$

where the impedances of the resonators are

$$Z_j(\omega) = \frac{1}{-i\omega C_{c,j}} - iZ_0 \tan\left(\frac{\pi}{2}\frac{\omega}{\omega_j} + i\alpha\right), \tag{5}$$

$$\alpha = \frac{1}{2}\ln\frac{Z_0 + R}{Z_0 - R}, \tag{6}$$

and the impedance of the SQUID is

$$Z_J(\omega, \Phi) = -i\omega L_J(\Phi) = \frac{-i\hbar\omega}{2eI_C(\Phi)}. \tag{7}$$

In Eq. (5) the angular frequencies ω_j correspond to the fundamental modes of the uncoupled resonators.

In Figs. 2 and 3 we plot, respectively, the transmission probability Eq. (4) and the heat current Eq. (3) evaluated numerically. In Fig. 3 the heat flux [Fig. 3(a)] and its modulation amplitude [Fig. 3(b)] are plotted versus the coupling strength between the SQUID and the resonators g defined in Eq. (25). Figure 3(b) illustrates the nonmonotonous dependence of the modulation amplitude $\Delta J(g)$. For the numerical
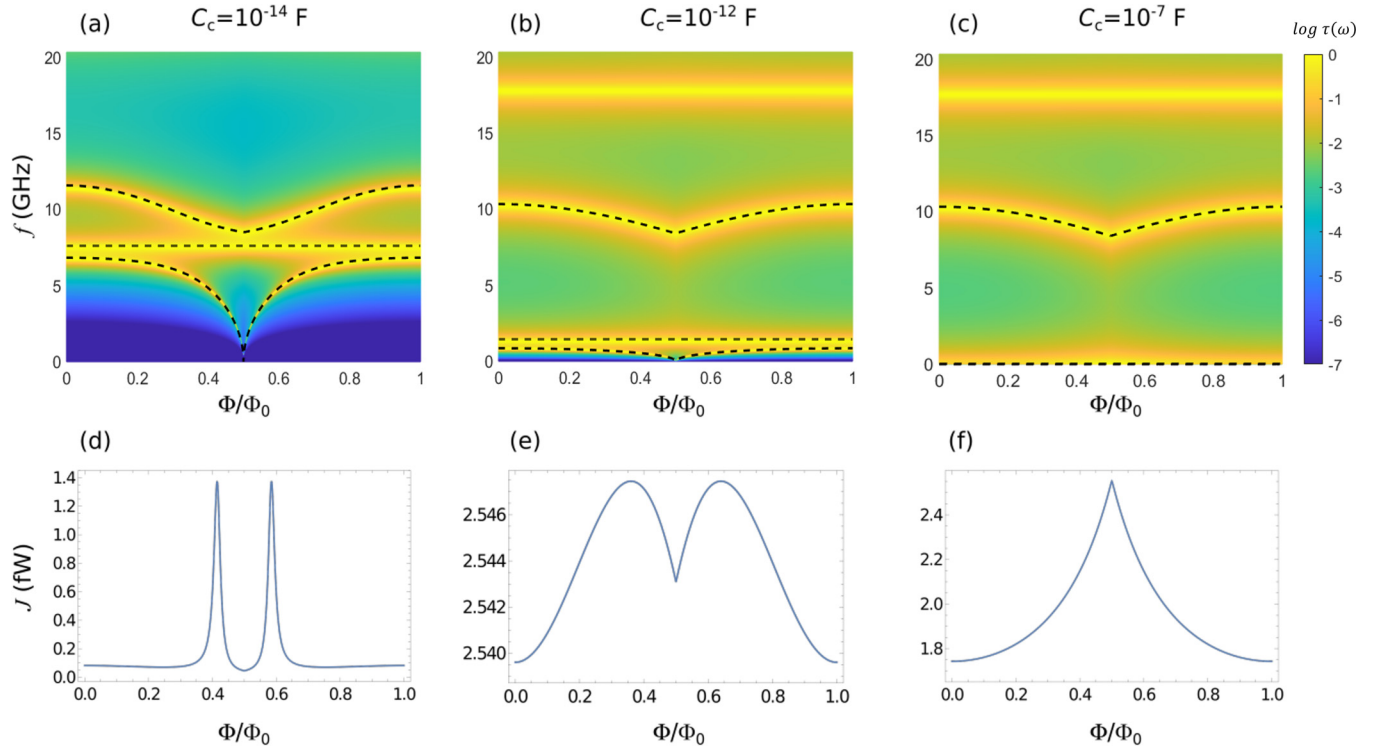
FIG. 2. Transmission probability and heat current in a symmetric system with $C_{c,1} = C_{c,2} = C_c$ and $\omega_1 = \omega_2$. Panels (a), (b), and (c)—transmission probability (4) versus normalized magnetic flux Φ/Φ_0 and the frequency $f = \omega/2\pi$. The black dashed lines are eigenfrequencies obtained from three-level system approximation, i.e., Eqs. (27) and (28). Panels (d), (e), and (f)—heat current (3) as a function of Φ/Φ_0. (a),(d) Weak coupling regime with $C_c = 10$ fF. The corresponding value of the coupling constant (11) is $g/2\pi = 296$ MHz, of the shifted resonator frequency (10) is $\Omega_r/2\pi = 8.73$ GHz, and of the damping rate (26) is $\kappa/2\pi = 451$ MHz. (b),(e) Intermediate coupling regime with $C_c = 1$ pF, the coupling constant (25) $g/2\pi = 2.592$ GHz, the frequency of the uncoupled mode (27) $\omega_{\mathrm{unc}}/2\pi = 4.15$ GHz, and the frequency of the coupled mode (24) $\Omega_r/2\pi = 8.425$ GHz and $\kappa/2\pi = 451$ MHz. (c),(f) Strong coupling regime with $C_c = 10^{-7}$ F, $g/2\pi = 2.975$ GHz, $\omega_{\mathrm{unc}}/2\pi = 14.87$ MHz, $\Omega_r/2\pi = 8.414$ GHz, and $\kappa/2\pi = 451$ MHz.

simulations we have used the parameter values typical for the experiment (see, e.g., Refs. [38,51,52]): $Z_0 = 50\,\Omega$, $R = 2\,\Omega$, $\omega_1/2\pi = \omega_2/2\pi = 8.84$ GHz, $C = 58.7$ fF, $I_C = 291$ nA, $T_2 = 300$ mK, and $T_1 = 150$ mK. The ratio between the Josephson energy and the maximum value of the charging energy achieved at $C_{c,1} = C_{c,2} = 0$, $\max(E_C) = e^2/2C$, is high, $E_J/\max(E_C) = 438$. For these parameters the replacement of the nonlinear SQUID by a linear inductor is justified. In the subsequent sections we discuss various approximate approaches, which allow us to find analytical expressions for the heat current and to understand the physics behind the unusual dependence $\Delta J(g)$.

III. QUALITATIVE DISCUSSION

The transmission probability Eq. (4) has peaks at frequencies corresponding to the eigenmodes of the whole system "two resonators plus SQUID." The position, the height, and the width of these peaks depend on magnetic flux. In Fig. 2 we plot the function $\tau(\omega, \Phi)$ for three different values of the coupling strength between the SQUID and the resonators. In this figure and in the rest of the paper, we assume that the maximum value of the SQUID frequency satisfies

$$\hbar\omega_{1,2} < \omega_J(0) < 3\hbar\omega_{1,2}. \tag{8}$$

In this case, the SQUID frequency [Eq. (2)] crosses only the lowest resonator modes.

In the weak coupling limit [Fig. 2(a)] the modes of the resonators and of the SQUID are almost independent. They become hybridized only in the vicinity of the flux point where $\omega_J(\Phi)$ crossed the frequency of the resonators $\omega_{1,2}$. The heat current through the system $J(\Phi)$ shows sharp peak at this point and almost vanishes away from it [Fig. 2(d)]. That is why the modulation of the heat current in the weak coupling limit approximately equals its maximum value. For the parameters chosen for the simulations, which are given above, the weak coupling limit is valid for $C_c \lesssim 50$ fF. A more general condition for this is given by Eq. (21).

At the intermediate coupling [Fig. 2(b)], the hybridization between the resonators and the SQUID becomes significant even far away from the crossing flux point. For this reason, the heat current peaks become broad and overlap [Fig. 2(e)]. Therefore, the magnitude of the heat current modulation drops. In fact, it almost vanishes; see Fig. 3(b). Another effect, visible in Fig. 2(b), is the splitting of the resonator modes into pairs. In each pair, only one of the modes is coupled to the SQUID and sensitive to the magnetic flux. Namely, it is the mode having voltage antinode in the vicinity of the SQUID and having the higher frequency of the two modes. In this regime, the coupling capacitors C_c are on the same order of magnitude as the effective capacitance of the resonators C_r,
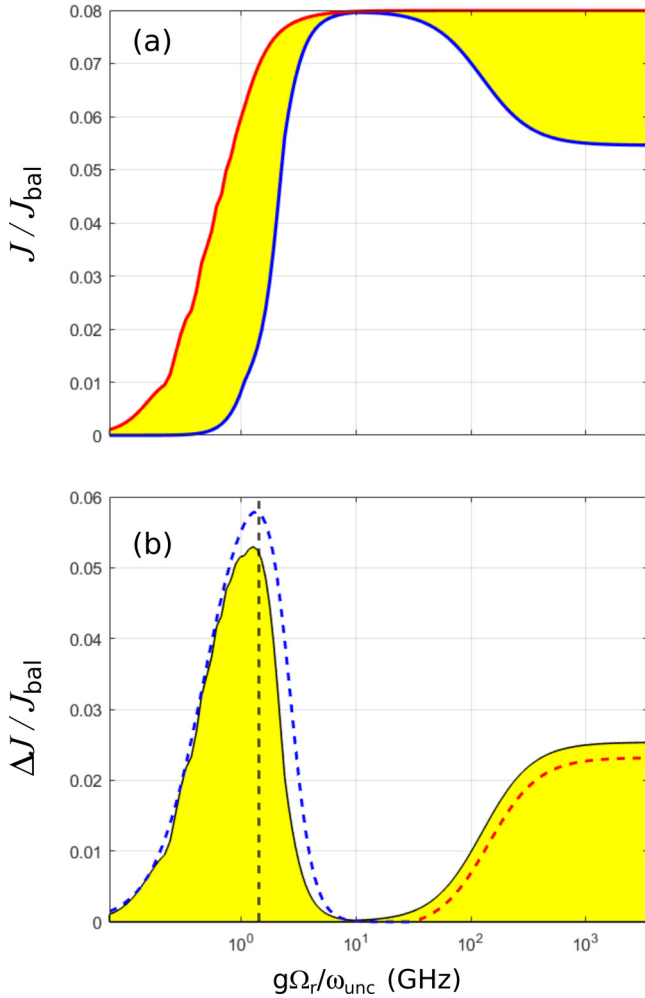
FIG. 3. Heat current (3) and heat current modulation amplitude ΔJ versus the coupling strength g (25). (a) The maximum (red line) and the minimum (blue line) photonic heat power (3) as a function of the coupling strength g. (b) The heat power modulation $\Delta J = J_{max} - J_{min}$. In both plots we have normalized the heat power by ballistic heat conduction, $J_{bal} = (\pi k_B^2 / 12\hbar)(T_2^2 - T_1^2)$, which follows from Eq. (3) if $\tau(\omega) \equiv 1$. For visual clarity, the horizontal axis shows the rescaled coupling strength $g\Omega_r/\omega_{unc}$. In panel (b) we also show the analytical approximations based on Eq. (29) (dashed blue line) and Eqs. (39) and (40) (dashed red line). Vertical black dashed line shows the predicted optimal coupling strength $g \approx \sqrt{\kappa \Omega_r/2}$, which follows from the condition (30) assuming $g \gtrsim \kappa/2$.

which will be defined below. In our simulation the intermediate coupling occurs in the range 50 fF $\lesssim C_c \lesssim$ 10 pF.

In the strong coupling regime [Fig. 2(c)] the two lowest lines in the spectrum move to very low frequencies. In this limit, the heat current modulation reappears again. In part, this effect is caused by the divergence of the Bose functions at low frequencies, which makes the relative contribution of these frequencies to the integral [Eq. (3)] more significant. In addition to that, the third hybrid mode with the frequency close to $\omega_{1,2}$ depends on the flux and also contributes to the modulation shown in Fig. 2(f). In this limit the coupling capacitors C_c are much larger than the effective capacitance

of the resonators C_r. For the parameters of our simulations it means $C_c \gtrsim$ 10 pF.

In the next three sections we discuss each of the regimes introduced above in detail.

IV. WEAK COUPLING REGIME

In the weak coupling regime, the Hamiltonian of the combined system "resonators plus SQUID" can be approximately reduced to that of three coupled oscillators [9,53,54],

$$H = \sum_{j=1,2} \hbar\Omega_j \left(a_j^\dagger a_j + \frac{1}{2} \right) + \hbar\omega_J(\Phi) \left(b^\dagger b + \frac{1}{2} \right)$$
$$- i\hbar g_1(a_1^\dagger - a_1)(b^\dagger + b) - i\hbar g_2(a_2^\dagger - a_2)(b^\dagger + b). \quad (9)$$

Here Ω_j are the frequencies of the two lowest modes of the resonators shifted by the presence of the capacitors $C_{c,j}$,

$$\Omega_j = \frac{\sqrt{\pi}\omega_j}{\sqrt{\pi + 4\omega_j Z_0 C_{c,j}}}, \quad (10)$$

a_j are the ladder operators of the resonators, b is the ladder operator of the SQUID, and

$$g_j = \sqrt{\frac{Z_0 C_{c,j}^2 \omega_j^3}{\pi(C_{c,1} + C_{c,2} + C)}} \quad (11)$$

are the coupling constants between the resonators and the SQUID.

In the rest of the paper we consider the symmetric case of two resonators with equal renormalized frequencies (10), $\Omega_1 = \Omega_2 = \Omega_r$. For such symmetric setup the heat current reaches the maximum values. To achieve the equality $\Omega_1 = \Omega_2$ for the asymmetric coupling with $C_{c,1} \neq C_{c,2}$, we adjust the frequencies ω_j accordingly. Equations (10) and (11) have been derived by expanding the tangents in the resonator impedances Eq. (5) as

$$\tan x = \sum_{n=0}^{\infty} \frac{2x}{\pi^2 \left(n + \frac{1}{2}\right)^2 - x^2} \quad (12)$$

and keeping only the pole in the expansion with $n = 0$. Equations (9)–(11) are valid at small coupling $g_j \ll \Omega_r$. Below we provide a more accurate condition for the weak coupling approximation, which also involves the damping rate of the resonators Eq. (21).

Determining the normal modes of the Hamiltonian Eq. (9), we find that one of them is independent of the magnetic flux because it is uncoupled from the SQUID. We call this mode "uncoupled"; it has a voltage node in the vicinity of the SQUID and in the weak coupling limit its frequency always equals that of the shifted resonator mode, $\omega_{unc} = \Omega_r$. The frequencies of the two other modes are

$$\omega_\pm = \sqrt{\frac{\Omega_r^2 + \omega_J^2 \pm \sqrt{\left(\Omega_r^2 - \omega_J^2\right)^2 + 16\left(g_1^2 + g_2^2\right)\Omega_r \omega_J}}{2}}. \quad (13)$$

In Fig. 2(a) these modes are clearly visible, while the uncoupled mode overlaps with $\omega_\pm$ due to the small value of the coupling constant g.

In the weak coupling limit the heat current Eq. (3) strongly increases at values of the magnetic flux Φ^*, which correspond to the resonance condition $\omega_J(\Phi^*) = \Omega_r$, and it almost vanishes away from this point [Fig. 2(d)]. In Fig. 2(a) the SQUID frequency crosses the resonator frequencies at the flux value $\Phi^* \approx 0.41\Phi_0$, where the heat modulation amplitude reaches the maximum value. To find the latter, it is sufficient to consider the range of frequencies $\omega \sim \omega_J \sim \Omega_r$, where one can accurately approximate the transmission probability Eq. (4) as follows:

$$\tau(\omega) = \frac{\kappa^2 g_1^2 g_2^2}{\left| (\omega - \omega_J)(\omega - \nu_r)^2 - (g_1^2 + g_2^2)(\omega - \nu_r) \right|^2}. \quad (14)$$

Here we have introduced the complex frequency $\nu_r = \Omega_r - i\kappa/2$, where

$$\kappa = \frac{4R\Omega_r}{\pi Z_0} \quad (15)$$

is the damping rate of the resonator modes.

The heat current Eq. (3) with the approximate transmission probability Eq. (14) can be evaluated analytically. If the temperatures of the resistors are sufficiently high, $k_B T_j \gtrsim |\omega_J - \Omega|$, we obtain

$$J(\Phi) = \frac{2g_1^2 g_2^2}{g_1^2 + g_2^2} \frac{\left(\frac{g_1^2 + g_2^2}{\kappa} + \frac{\kappa}{2} \right) \hbar \Omega_r [N_2(\Omega_r) - N_1(\Omega_r)]}{[\omega_J(\Phi) - \Omega_r]^2 + \left(\frac{g_1^2 + g_2^2}{\kappa} + \frac{\kappa}{2} \right)^2}. \quad (16)$$

The maximum of the heat flux is achieved at the resonance condition $\Phi = \Phi^*$,

$$J_{\max} = \frac{2g_1^2 g_2^2}{g_1^2 + g_2^2} \frac{\hbar \Omega_r [N_2(\Omega_r) - N_1(\Omega_r)]}{\frac{g_1^2 + g_2^2}{\kappa} + \frac{\kappa}{2}}, \quad (17)$$

while the minimum occurs far away from the resonance, i.e., either at zero flux, $\Phi = 0$, or at $\Phi = \Phi_0/2$. As we have discussed, at weak coupling one always has $J_{\min} \ll J_{\max}$. Therefore, in this regime the modulation of the heat current is close to its maximum value,

$$\Delta J = J_{\max} - J_{\min} \approx J_{\max}. \quad (18)$$

In the symmetric case $g_1 = g_2 = g$ and at very weak coupling $g \ll \kappa/2$ one finds

$$\Delta J = \frac{2g^2}{\kappa} \hbar \Omega_r [N_2(\Omega_r) - N_1(\Omega_r)]. \quad (19)$$

Thus, in this limit, the heat modulation grows with the coupling strength as g^2. In the limit $g \gg \kappa/2$ the modulation saturates at the value

$$\Delta J = \frac{\kappa}{2} \hbar \Omega_r [N_2(\Omega_r) - N_1(\Omega_r)]. \quad (20)$$

Considering ΔJ as a function of the damping rate κ at fixed g, we find that the optimal value of the damping rate is $\kappa_{\text{opt}} = 2g$ and the modulation amplitude at this point becomes $\Delta J_{\text{opt}} = (g/2) \hbar \Omega_r [N_2(\Omega_r) - N_1(\Omega_r)]$.

In Eq. (16) we have ignored the contributions of the high frequency modes of the resonators to the heat transport. Since in our model the SQUID angular frequency $\omega_J(\Phi)$ does not cross these modes, in the weak coupling regime they give small contribution.

In Fig. 3 we plot the maximum and the minimum values of the heat current and its modulation amplitude, obtained numerically, as a function of the coupling constant g and compare them with the approximate results. We note that the expressions Eqs. (17) and (18) well agree with the numerics in the weak coupling regime.

Finally, we provide a more accurate condition under which the weak coupling expressions Eqs. (16)–(20) are valid,

$$\frac{2g^2}{\kappa} + \frac{\kappa}{2} \lesssim |\omega_J(0) - \Omega_r| \lesssim \frac{k_B T_j}{\hbar}. \quad (21)$$

V. INTERMEDIATE COUPLING REGIME

In this section we consider the intermediate coupling regime $g_j \sim \Omega_r$. In this case, the expressions for the coupling constants g_j, Eq. (11), and for other parameters should be corrected. To obtain the corrected expressions, we consider the classical Lagrangian of the system. For simplicity, we consider a fully symmetric setup and put $\omega_1 = \omega_2 = \omega_r$, $C_{c,1} = C_{c,2} = C_c$, and $g_1 = g_2 = g$. We also define the effective capacitance of the $\lambda/4$ resonators, $C_r = \pi/4Z_0\omega_r$ (we obtain $C_r \approx 0.28$ pF for the simulation parameters given at the end of Sec. II), and their effective inductances $L_r = 4Z_0/\pi\omega_r$. Afterwards, the classical Lagrangian of the lowest modes of the resonators interacting with the SQUID is expressed as

$$\mathcal{L} = \frac{\hbar^2}{8e^2} \sum_{j=1,2} \left(C_r \dot{\varphi}_j^2 - \frac{\varphi_j^2}{L_r} + C_c (\dot{\varphi}_j - \dot{\varphi})^2 \right) + \frac{\hbar^2}{8e^2} \left(C\dot{\varphi} - \frac{2eI_C(\Phi)}{\hbar} \varphi^2 \right). \quad (22)$$

Here φ is the Josephson phase of the SQUID and φ_j are the phases describing the resonators. They are related to the electric potentials at the ends of the resonators, adjacent to the coupling capacitors, V_j, as $\dot{\varphi}_j = 2eV_j/\hbar$. Diagonalizing the Lagrangian Eq. (22), we obtain the corrected expressions for the angular Josephson frequency ω_J, for the angular frequencies of the resonator modes Ω_r, and for the coupling constant g:

$$\omega_J(\Phi) = \sqrt{\frac{2eI_C(\Phi)(C_r + C_c)}{\hbar[CC_c + (C + 2C_c)C_r]}}, \quad (23)$$

$$\Omega_r = \omega_r \sqrt{\frac{(C + 2C_c)C_r}{CC_c + (C + 2C_c)C_r}}, \quad (24)$$

$$g = \omega_r \sqrt{\frac{C_c^2 C_r}{4(C_r + C_c)[CC_c + (C + 2C_c)C_r]}}. \quad (25)$$

In the limit $C_c \ll C_r$ these expressions match the weak coupling formulas given in the previous section. In addition, if the resistance R approaches Z_0 one should use a more accurate expression for the damping rate,

$$\kappa = \frac{4RZ_0\omega_r}{\pi |Z_0^2 - R^2|}. \quad (26)$$

With these corrections, Eq. (16) approximately describes the heat current in the intermediate coupling regime. The frequencies of the eigenmodes of the coupled system in the limit

$R \to 0$ are

$$\omega_{\text{unc}} = \omega_r \sqrt{\frac{C_r}{C_r + C_c}} \qquad (27)$$

for the mode uncoupled from the SQUID and

$$\omega_{\pm} = \sqrt{\frac{\Omega_r^2 + \omega_J^2 \pm \sqrt{(\Omega_r^2 - \omega_J^2)^2 + 32g^2\omega_J^2}}{2}} \qquad (28)$$

for the two hybrid modes. Note that the interaction term in this equation slightly differs from that in Eq. (13). As expected, in the limit $C_c \ll C_r$ these expressions match those of the previous section.

The main difference between the weak and the intermediate coupling regimes is in the growing value of the minimum heat current. Assuming that $J_{\text{min}} = J(0)$, from Eq. (16) one finds the modulation in the form

$$\Delta J = \frac{g^2 [\omega_J(0) - \Omega_r]^2 \hbar \Omega_r [N_2(\Omega_r) - N_1(\Omega_r)]}{\left[[\omega_J(0) - \Omega_r]^2 + \left(\frac{2g^2}{\kappa} + \frac{\kappa}{2} \right)^2 \right] \left(\frac{2g^2}{\kappa} + \frac{\kappa}{2} \right)}. \qquad (29)$$

This modulation amplitude significantly drops if

$$\frac{2g^2}{\kappa} + \frac{\kappa}{2} \gtrsim |\omega_J(0) - \Omega_r|, \qquad (30)$$

i.e., as soon as the coupling can no longer be considered weak. As in the weak coupling regime, the optimal damping rate ensuring the strongest modulation is $\kappa_{\text{opt}} = 2g$. With this condition fulfilled, the amplitude (29) takes the maximum value ΔJ_{max} at the coupling strength $g_{\text{opt}} \approx |\omega_J(0) - \Omega_r|/2$. Thus we estimate the strongest possible heat modulation as

$$\Delta J_{\text{max}} \approx \frac{|\omega_J(0) - \Omega_r|}{8} \hbar \Omega_r [N_2(\Omega_r) - N_1(\Omega_r)]. \qquad (31)$$

At these optimal conditions the quality factor of the resonators $Q_{\text{opt}} = \Omega_r / 2g_{\text{opt}} = \Omega_r / |\omega_J(0) - \Omega_r|$ is low if the SQUID frequency $\omega_J(0)$ is far detuned from Ω_r.

To illustrate these points, in Fig. 2(b) we show the transmission probability $\tau(\omega, \Phi)$ in the intermediate coupling regime $g \sim \Omega_r$. The flux-independent line at $f \approx 4.4$ GHz corresponds to the uncoupled mode of Eq. (27). The lines corresponding to hybrid modes of Eq. (28) are well separated at all values of magnetic flux. This is why the dependence of the heat current on Φ becomes weak and does not exhibit a resonance peak [Fig. 2(e)]. This, in turn, suppresses the heat current modulation, as it is evident from Fig. 3(b) for the range of couplings $1 \text{ GHz} \lesssim g\Omega_r/\omega_{\text{unc}} \lesssim 100 \text{ GHZ}$.

VI. STRONG COUPLING REGIME

In the strong coupling limit the hybrid mode $\omega_-(\Phi)$ [Eq. (28)] and the uncoupled mode ω_{unc} [Eq. (27)] move to low frequencies, where they merge and form a broad peak in transmission probability, which is sensitive to the magnetic flux. The mode $\omega_+(\Phi)$ becomes isolated, with pronounced dependence on the magnetic flux due to its strong coupling to the SQUID; see Fig. 2(c). These effects lead to the reappearance of the heat current modulation in the strong coupling limit.

The formal condition for the strong coupling limit, where one can derive simple approximate expressions, is

$$C_c \gg \max\{C_r, C, L_r/R^2\}. \qquad (32)$$

In the limit $C_c \gg \max\{C_r, C\}$ Eqs. (23)–(25) become

$$\omega_J(\Phi) = \sqrt{\frac{2e\hbar I_C(\Phi)}{C + 2C_r}}, \qquad (33)$$

$$\Omega_r = \omega_r \sqrt{\frac{2C_r}{C + 2C_r}}, \quad g = \omega_r \sqrt{\frac{C_r}{4(C + 2C_r)}}. \qquad (34)$$

Furthermore, at low frequencies $\omega \ll \omega_r$ one can approximate the impedances of the resonators Eq. (5) as $Z_1(\omega) = Z_2(\omega) = -i\omega L_r + R$. In this limit, at small capacitance of the SQUID, $C \ll L_r/R^2$ and for $C_c \gg L_r/R^2$ the transmission probability at low frequencies acquires the form of a non-Lorentzian peak,

$$\tau(\omega) = \frac{4R^2\omega^2}{\left(\frac{2eI_C(\Phi)}{\hbar}(\omega^2 L_r^2 + R^2) + 2\omega^2 L_r \right)^2 + 4R^2\omega^2}. \qquad (35)$$

This peak has a maximum at frequency $\omega_{\text{max}} \sim R/L_r$. The contribution of the low frequency peak to the heat flux can be evaluated analytically for temperatures $T_1, T_2 \gtrsim \hbar R/k_B L_r$. In this case, in Eq. (3) one can make the low frequency approximation for the Bose functions

$$\hbar\omega[N_2(\omega) - N_1(\omega)] \to k_B(T_2 - T_1). \qquad (36)$$

After that, Eq. (3) with the transmission probability Eq. (35) leads to the contribution to the heat flux coming from the low frequency peak in the form

$$J_l(\Phi) = \frac{\kappa k_B(T_2 - T_1)}{4[1 + A(\Phi)][2 + A(\Phi)]}. \qquad (37)$$

Here we have defined the flux dependent dimensionless parameter

$$A(\Phi) = \frac{\pi e Z_0 I_C(\Phi)}{\hbar\omega_r} = \frac{\pi^2}{8} \frac{L_r}{L_J(\Phi)}. \qquad (38)$$

One can work out an even more accurate approximation for the low frequency contribution,

$$J_l(\Phi) = \frac{\kappa k_B(T_2 - T_1)}{4[2 + A(\Phi)]} \frac{A(\Phi)\kappa^2 + 4[1 + A(\Phi)]\omega_{\text{unc}}^2}{A(\Phi)[1 + A(\Phi)]\kappa^2 + 4\omega_{\text{unc}}^2}. \qquad (39)$$

This result can be extended to the intermediate coupling regime, i.e., to the values of C_c smaller than the condition Eq. (32) requires.

The contribution of the mode ω_+ [Eq. (28)] to the heat current can be estimated as

$$J_+(\Phi) = \frac{\kappa}{4} \hbar\omega_+(\Phi)\{N_2[\omega_+(\Phi)] - N_1[\omega_+(\Phi)]\}, \qquad (40)$$

where the frequency $\omega_+(\Phi)$ is given by Eq. (28). In the limit $C_c \gg \max\{C_r, C\}$, where $g^2 = \Omega_r^2/8$, this frequency acquires a simple form

$$\omega_+(\Phi) = \sqrt{\Omega_r^2 + \omega_J^2(\Phi)}$$

$$= \sqrt{\omega_r^2 \frac{2C_r}{C + 2C_r} + \frac{2eI_C(\Phi)}{\hbar(C + 2C_r)}}. \qquad (41)$$

The total heat current takes the form

$$J(\Phi) = J_l(\Phi) + J_+(\Phi) + J_{\mathrm{bg}}(\Phi), \qquad (42)$$

where $J_{\mathrm{bg}}(\Phi)$ is the background contribution coming from the modes with frequencies higher than ω_+. Interestingly, in the strong coupling regime the heat current has a maximum at $\Phi = 0.5\Phi_0$ and minimum at $\Phi = 0$; see Fig. 2(f).

In Figs. 3(a) and 3(b) we observe the reappearance of the heat current modulation at strong coupling. For the chosen parameters the modulation predominantly comes from the term $J_+(\Phi)$ [Eq. (40)], although the low frequency part $J_l(\Phi)$ also gives nonvanishing contribution. In the limit $C_c \to \infty$ and for $k_B T_{1,2} \gtrsim \omega_+(\Phi)$ the modulation approaches the limiting value

$$\Delta J = \left[\frac{A(1+A)}{(1+A)(2+A)} + \frac{\hbar^2 \omega_+^2}{6k_B^2 T_1 T_2} \right] \frac{\kappa k_B (T_2 - T_1)}{8}, \qquad (43)$$

where both A and ω_+ are taken at $\Phi = 0$.

VII. CONCLUSION

In conclusion, we have studied photonic heat transport through a SQUID coupled to the two resonators and two resistors. By tuning the critical current of the SQUID with magnetic flux, one can control the heat power transmitted from the hot resistor to the cold one. This device can be used as a heat valve provided its parameters are chosen properly. We study the performance of the heat valve depending on the coupling strength between the resonators and the SQUID. We find that the main parameter characterizing the performance of such device, namely, the amplitude of modulation of the photonic heat power, nonmonotonously varies with the coupling strength. The modulation grows with the coupling strength in the weak coupling regime, then significantly drops at the intermediate coupling, and, finally, it reappears again in the strong coupling limit. This unusual behavior is explained by the resonant nature of the heat transport in the system. Indeed, at weak coupling the heat flows through the device only at magnetic flux values corresponding to the resonance condition $\omega_J(\Phi) = \Omega_r$ and drops to zero away from these values. As a result, the dependence of the heat power on the magnetic flux, $J(\Phi)$, is given by a periodic set of narrow peaks. At the intermediate coupling these peaks become broader and eventually overlap, thus reducing the heat modulation. The optimal performance of the heat valve is achieved at the boundary between the weak and the intermediate coupling regimes and at the resonator damping rates close to the coupling constant between resonators and the SQUID. Our results can help to optimize the design of the low temperature heat valves based on superconducting circuit components.
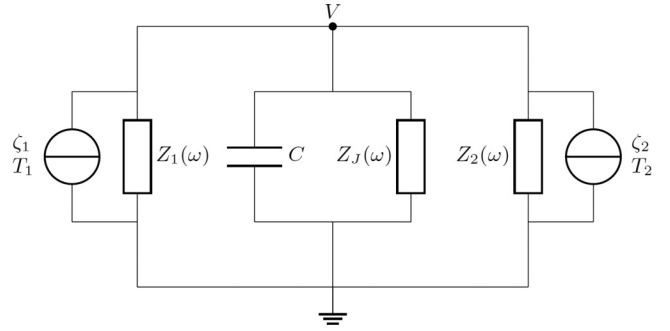
ACKNOWLEDGMENTS

FIG. 4. Equivalent lumped-element circuit of the system shown in Fig. 1 with the SQUID has been replaced by a linear lumped element with the impedance $Z_J(\omega)$. The resistors generate the noise currents ζ_1 and ζ_2, which carry the information about the temperature T_1 and T_2.

APPENDIX: DERIVATION OF EQ. (4)

In this Appendix we provide the derivation of the transmission probability (4) following the method of Ref. [43]. Kirchhoff's equations for the circuit of Fig. 4 read

$$I_1(t) = \int_{-\infty}^{t} dt' Y_1(t - t') V(t') + \zeta_1(t), \qquad (A1)$$

$$I_2(t) = \int_{-\infty}^{t} dt' Y_2(t - t') V(t') + \zeta_2(t), \qquad (A2)$$

$$I_J(t) = C\dot{V} + I_C \sin\varphi, \quad I_1(t) + I_2(t) + I_J(t) = 0. \qquad (A3)$$

Here the admittances of the environment 1 and 2 in the time domain are defined as $Y_j(t) = \int d\omega \, e^{-i\omega t}/[2\pi Z_j(\omega)]$. The voltage drop across the junction is related to the phase by the second Josephson relation $V = \hbar\dot{\varphi}/2e$. The noises ζ_1 and ζ_2 are the Gaussian stochastic processes fully characterized by their pair correlators

$$\langle \zeta_i(t')\zeta_j(t'') \rangle = \int \frac{d\omega}{2\pi} \langle |\zeta_j|_\omega^2 \rangle \cos[\omega(t' - t'')]\delta_{ij}, \qquad (A4)$$

$$\langle |\zeta_j|_\omega^2 \rangle = \mathrm{Re}\left[\frac{1}{Z_j(\omega)} \right] \hbar\omega \coth\frac{\hbar\omega}{2k_b T_j}. \qquad (A5)$$

The heat current flowing through the circuit is given by the Joule heating in the impedance $Z_1(\omega)$ averaged over the noises ζ_j

$$J = \langle I_1 V \rangle_\zeta. \qquad (A6)$$

After linearizing the SQUID dynamics, i.e., replacing $\sin\varphi$ by φ, one can replace it by an inductor. Afterwards, the current across the junction in Fourier domain becomes $V_\omega/Z_J(\omega)$. Solving Eqs. (A1), (A2), and (A3) in Fourier domain, we obtain the Fourier component of the voltage in the form

$$V_\omega = -\frac{\zeta_{1,\omega} + \zeta_{2,\omega}}{-i\omega C + \frac{1}{Z_1(\omega)} + \frac{1}{Z_2(\omega)} + \frac{1}{Z_J(\omega)}}. \qquad (A7)$$

The heat flux Eq. (A6) now reads

$$
\begin{aligned}
J &= \int \frac{d\omega}{2\pi} \langle I_{1,\omega} V_{-\omega} \rangle_\zeta \\
&= \int \frac{d\omega}{2\pi} \left\langle \left(\frac{V_\omega}{Z_1(\omega)} + \zeta_{1,\omega} \right) V_{-\omega} \right\rangle_\zeta \\
&= \int_0^\infty \frac{d\omega}{2\pi} \frac{2\,\mathrm{Re}\left[\frac{\langle |\zeta_2|_\omega^2 \rangle}{Z_1} - \frac{\langle |\zeta_1|_\omega^2 \rangle}{Z_2} \right]}{\left| -i\omega C + \frac{1}{Z_1(\omega)} + \frac{1}{Z_2(\omega)} + \frac{1}{Z_J(\omega)} \right|^2}.
\end{aligned}
\tag{A8}
$$

Using the spectral power of the noises (A5), one can show that the above expression is equivalent to Eq. (3) with the transmission probability given by Eq. (4).

---

[1] S. Deffner and S. Campbell, *Quantum Thermodynamics* (Morgan and Claypool Publishers, San Rafael, CA, 2019), pp. 2053–2571.

[2] P. Strasberg and A. Winter, First and second law of quantum thermodynamics: A consistent derivation based on a microscopic definition of entropy, PRX Quantum **2**, 030202 (2021).

[3] N. M. Myers, O. Abah, and S. Deffner, Quantum thermodynamic devices: from theoretical proposals to experimental reality, AVS Quantum Sci. **4**, 027101 (2022).

[4] A. Dhar and D. Roy, Heat transport in harmonic lattices, J. Stat. Phys. **125**, 801 (2006).

[5] A. Dhar, Heat transport in low-dimensional systems, Adv. Phys. **57**, 457 (2008).

[6] Y. Dubi and M. Di Ventra, Colloquium: Heat flow and thermoelectricity in atomic and molecular junctions, Rev. Mod. Phys. **83**, 131 (2011).

[7] N. Li, J. Ren, L. Wang, G. Zhang, P. Hänggi, and B. Li, Colloquium: Phononics: Manipulating heat flow with electronic analogs and beyond, Rev. Mod. Phys. **84**, 1045 (2012).

[8] N. Mosso, U. Drechsler, F. Menges, P. Nirmalraj, S. Karg, H. Riel, and B. Gotsmann, Heat transport through atomic contacts, Nat. Nanotechnol. **12**, 430 (2017).

[9] G. Thomas, J. P. Pekola, and D. S. Golubev, Photonic heat transport across a Josephson junction, Phys. Rev. B **100**, 094508 (2019).

[10] J. P. Pekola and B. Karimi, Colloquium: Quantum heat transport in condensed matter systems, Rev. Mod. Phys. **93**, 041001 (2021).

[11] H. E. D. Scovil and E. O. Schulz-DuBois, Three-Level Masers as Heat Engines, Phys. Rev. Lett. **2**, 262 (1959).

[12] O. Abah, J. Rossnagel, G. Jacob, S. Deffner, F. Schmidt-Kaler, K. Singer, and E. Lutz, Single-Ion Heat Engine at Maximum Power, Phys. Rev. Lett. **109**, 203006 (2012).

[13] R. Uzdin, A. Levy, and R. Kosloff, Equivalence of Quantum Heat Machines, and Quantum-Thermodynamic Signatures, Phys. Rev. X **5**, 031044 (2015).

[14] G. Benenti, G. Casati, K. Saito, and R. Whitney, Fundamental aspects of steady-state conversion of heat to work at the nanoscale, Phys. Rep. **694**, 1 (2017).

[15] K. Brandner, M. Bauer, and U. Seifert, Universal Coherence-Induced Power Losses of Quantum Heat Engines in Linear Response, Phys. Rev. Lett. **119**, 170602 (2017).

[16] M. Campisi and R. Fazio, The power of a critical heat engine, Nat. Commun. **7**, 11895 (2016).

[17] I. Díaz and R. Sánchez, The qutrit as a heat diode and circulator, New J. Phys. **23**, 125006 (2021).

[18] D. Segal and A. Nitzan, Spin-Boson Thermal Rectifier, Phys. Rev. Lett. **94**, 034301 (2005).

[19] T. Ruokola, T. Ojanen, and A.-P. Jauho, Thermal rectification in nonlinear quantum circuits, Phys. Rev. B **79**, 144306 (2009).

[20] B. Bhandari, P. A. Erdman, R. Fazio, E. Paladino, and F. Taddei, Thermal rectification through a nonlinear quantum resonator, Phys. Rev. B **103**, 155434 (2021).

[21] D. Goury and R. Sánchez, Reversible thermal diode and energy harvester with a superconducting quantum interference single-electron transistor, Appl. Phys. Lett. **115**, 092601 (2019).

[22] T. Ojanen and A.-P. Jauho, Mesoscopic Photon Heat Transistor, Phys. Rev. Lett. **100**, 155902 (2008).

[23] K. Joulain, J. Drevillon, Y. Ezzahri, and J. Ordonez-Miranda, Quantum Thermal Transistor, Phys. Rev. Lett. **116**, 200601 (2016).

[24] M. Majland, K. S. Christensen, and N. T. Zinner, Quantum thermal transistor in superconducting circuits, Phys. Rev. B **101**, 184510 (2020).

[25] N. Ligato, F. Paolucci, E. Strambini, and F. Giazotto, Thermal superconducting quantum interference proximity transistor, Nat. Phys. **18**, 627 (2022).

[26] G. Thomas, A. Gubaydullin, D. S. Golubev, and J. P. Pekola, Thermally pumped on-chip maser, Phys. Rev. B **102**, 104503 (2020).

[27] J. P. Pekola, Towards quantum thermodynamics in electronic circuits, Nat. Phys. **11**, 118 (2015).

[28] K. Maki and A. Griffin, Entropy Transport Between Two Superconductors by Electron Tunneling, Phys. Rev. Lett. **15**, 921 (1965).

[29] P. Virtanen and T. Heikklä, Thermoelectric effects in superconducting proximity structures, Appl. Phys. A **89**, 625 (2007).

[30] J. Eom, C.-J. Chien, and V. Chandrasekhar, Phase Dependent Thermopower in Andreev Interferometers, Phys. Rev. Lett. **81**, 437 (1998).

[31] A. Parsons, I. A. Sosnin, and V. T. Petrashov, Reversal of thermopower oscillations in the mesoscopic Andreev interferometer, Phys. Rev. B **67**, 140502(R) (2003).

[32] Z. Jiang and V. Chandrasekhar, Quantitative measurements of the thermal resistance of Andreev interferometers, Phys. Rev. B **72**, 020502(R) (2005).

[33] F. Giazotto and M. J. Martínez-Pérez, The Josephson heat interferometer, Nature (London) **492**, 401 (2012).

[34] E. Strambini, F. S. Bergeret, and F. Giazotto, Proximity nanovalve with large phase-tunable thermal conductance, Appl. Phys. Lett. **105**, 082601 (2014).

[35] M. Meschke, W. Guichard, and J. P. Pekola, Single-mode heat conduction by photons, Nature (London) **444**, 187 (2006).

[36] A. V. Timofeev, M. Helle, M. Meschke, M. Möttönen, and J. P. Pekola, Electronic Refrigeration at the Quantum Limit, Phys. Rev. Lett. **102**, 200801 (2009).

[37] M. Partanen, K. Y. Tan, J. Govenius, R. E. Lake, M. K. Mäkelä, T. Tanttu, and M. Möttönen, Quantum-limited heat conduction over macroscopic distances, Nat. Phys. **12**, 460 (2016).

[38] A. Ronzani, B. Karimi, J. Senior, Y.-C. Chang, J. T. Peltonen, C. Chen, and J. P. Pekola, Tunable photonic heat transport in a quantum heat valve, Nat. Phys. **14**, 991 (2018).

[39] M. Xu, J. T. Stockburger, and J. Ankerhold, Heat transport through a superconducting artificial atom, Phys. Rev. B **103**, 104304 (2021).

[40] D. R. Schmidt, R. J. Schoelkopf, and A. N. Cleland, Photon-Mediated Thermal Relaxation of Electrons in Nanostructures, Phys. Rev. Lett. **93**, 045901 (2004).

[41] F. Giazotto, T. T. Heikkilä, A. Luukanen, A. M. Savin, and J. P. Pekola, Opportunities for mesoscopics in thermometry and refrigeration: Physics and applications, Rev. Mod. Phys. **78**, 217 (2006).

[42] A. Schmid, On a quasiclassical Langevin equation, J. Low Temp. Phys. **49**, 609 (1982).

[43] L. M. A. Pascal, H. Courtois, and F. W. J. Hekking, Circuit approach to photonic heat transport, Phys. Rev. B **83**, 125113 (2011).

[44] F. Paolucci, G. Timossi, P. Solinas, and F. Giazotto, Coherent manipulation of thermal transport by tunable electron-photon and electron-phonon interaction, J. Appl. Phys. **121**, 244305 (2017).

[45] D. Segal, Heat flow in nonlinear molecular junctions: Master equation analysis, Phys. Rev. B **73**, 205415 (2006).

[46] L. Nicolin and D. Segal, Quantum fluctuation theorem for heat exchange in the strong coupling regime, Phys. Rev. B **84**, 161414(R) (2011).

[47] C. Wang, J. Ren, and J. Cao, Nonequilibrium energy transfer at nanoscale: A unified theory from weak to strong coupling, Sci. Rep. **5**, 11787 (2015).

[48] D. He, J. Thingna, and J. Cao, Interfacial thermal transport with strong system-bath coupling: A phonon delocalization effect, Phys. Rev. B **97**, 195437 (2018).

[49] D. Xu and J. Cao, Non-canonical distribution and nonequilibrium transport beyond weak system-bath coupling regime: A polaron transformation approach, Front. Phys. **11**, 110308 (2016).

[50] P. Talkner and P. Hänggi, Colloquium: Statistical mechanics and thermodynamics at strong coupling: Quantum and classical, Rev. Mod. Phys. **92**, 041002 (2020).

[51] A. Gubaydullin, G. Thomas, D. S. Golubev, D. Lvov, J. T. Peltonen, and J. P. Pekola, Photonic heat transport in three terminal superconducting circuit, Nat. Commun. **13**, 1552 (2022).

[52] A. Guthrie, C. Dimas Satrya, Y.-C. Chang, P. Menczel, F. Nori, and J. P. Pekola, Cooper-Pair Box Coupled to Two Resonators: An Architecture for a Quantum Refrigerator, Phys. Rev. Appl. **17**, 064022 (2022).

[53] J. Koch, T. M. Yu, J. Gambetta, A. A. Houck, D. I. Schuster, J. Majer, A. Blais, M. H. Devoret, S. M. Girvin, and R. J. Schoelkopf, Charge-insensitive qubit design derived from the Cooper pair box, Phys. Rev. A **76**, 042319 (2007).

[54] D. S. Golubev, E. V. Ilíchev, and L. S. Kuzmin, Single-Photon Detection with a Josephson Junction Coupled to a Resonator, Phys. Rev. Appl. **16**, 014025 (2021).